Supporting Information

For

Carboxylate Structural Effects on the Properties and Proton-Coupled Electron Transfer Reactivity of $[CuO_2CR]^{2+}$ Cores.

Courtney E. Elwell,[a] Mukunda Mandal,[a] Caitlin J. Bouchey,[a,b] Lawrence Que, Jr.,[a] Christopher J. Cramer,[a,*] and William B. Tolman[b,*]

[a]Department of Chemistry, Center for Metals in Biocatalysis, Chemical Theory Center, and Supercomputing Institute, University of Minnesota, 207 Pleasant Street SE, Minneapolis, Minnesota, 55455, United States.

[b]Department of Chemistry, Washington University in St. Louis, One Brookings Drive, Campus Box 1134, St. Louis, Missouri 63130, United States.

*Corresponding authors: wbtolman@wustl.edu, cramer@umn.edu

Table of Contents

1. Experimental materials and methods.

Preparation and handling of the air-sensitive compounds were carried out under a dinitrogen atmosphere either in a glove-box or using Schlenk techniques. All reagents and solvents were purchased from commercial sources and used as received unless otherwise noted. Diethyl ether, pentane and tetrahydrofuran were passed through solvent purification columns (Glass Contour, Laguna, California). 1,2-difluorobenzene (DFB) was dried over calcium hydride powder and basic alumina, separately, and vacuum distilled. All solvents were stored over activated 3 Å molecular sieves in a N_2 filled glove-box prior to use. 1,4-Cyclohexadiene (CHD) was purchased from Sigma-Aldrich and dried over $MgSO_4$, degassed by three freeze-pump-thaw cycles, and vacuum transferred. The CHD was then brought into a nitrogen-filled glovebox, stored over activated 3 Å molecular sieves, and filtered using a 25 mm diameter, 0.2 μm hydrophobic polytetrafluoroethylene (PTFE) syringe filter before use. The compounds H_2L where L = N,N'-Bis(2,6-diisopropylphenyl)-2,6-pyridinecarboxamide,[1] $[NBu_4][LCu^{II}\text{-}OH]$[2] and acetylferrocenium tetrakis(3,5-bis(trifluoromethyl)phenyl)borate ($[AcFc][BAr^F{}_4]$)[3] were synthesized by published procedures. The compound $[NEt_4][LCu^{II}\text{-}OH]$ was prepared using the same procedure as reported for the synthesis of $[NBu_4][LCu^{II}\text{-}OH]$[2], except tetraethylammonium hydroxide was used instead of tetrabutylammonium hydroxide. 2,6-Diisopropylaniline (90%, technical grade), 2,6-pyridinedicarbonyl dichloride (97%), decamethylferrocene (Fc*, 97%), pentafluorobenzoic acid ($HO_2CC_6F_5$, 99%), 2,4,6-triisopropylbenzoic acid ($HO_2CC_6H_2(iPr_3)$, 97%), *p*-nitrobenzoic acid ($HO_2CC_6H_4(NO_2)$, 98%), benzoic acid ($HO_2CC_6H_5$, 97%), *p*-methoxybenzoic acid ($HO_2CC_6H_4(OMe)$, 98%) and tetrabutylammonium acetate ($NBu_4(O_2CCH_3)$, 97%) were procured from Sigma Aldrich Chemical Co. and used without further purification.

UV-vis spectra were collected on a HP8453 (190-1100 nm) diode array spectrophotometer. Low-temperature UV-vis experiments were performed using a Unisoku low-temperature UV-vis cell holder. EPR data were collected on a Bruker Elexsys E500 spectrophotometer using X-band radiation at 35 dB and 30 K. EPR spectral simulations were performed using EasySpin software (version 5.2.25).[4] Cyclic voltammograms were recorded using an EC Epsilon potentiostat from BASi, a glassy carbon working electrode and an Ag pseudoreference electrode. All cyclic

voltammograms were internally referenced to the either the ferrocene/ferrocenium (Fc/Fc^+) or decemethylferrocene/decamethylferrocenium (Fc^*/Fc^{*+}) couple.

For X-ray crystallography experiments, crystals were placed onto the tip of a 0.1 mm diameter mitogen polymer tip and mounted on a Bruker APEX II Platform CCD diffractometer for data collection. The data collections were carried out using MoKα radiation with a graphite monochromator (λ = 0.71073 Å) at 173 K. Structure solutions were performed by direct methods using SHELXS-2013 software and refined against F2 using full-matrix-least-squares using SHELXL-97 and SHELXL-2013 software.[5]

$[NBu_4][LCu^{II}(O_2CC_6F_5)]$. The synthesis of $[NBu_4][LCu^{II}(O_2CC_6F_5)]$ was adapted from the previously outlined synthesis of $[NBu_4][LCu^{II}(O_2CC_6H_4(Cl))]$.[6] A 25 mL Schlenk flask in a nitrogen filled glovebox at room temperature was charged with 120 mg (0.15 mmol) of solid $[NBu_4][LCu^{II}(OH)]$ and approximately 5 g of activated 3 Å molecular sieves. To this flask, ~8 mL of anhydrous THF was added, resulting in a blue solution. After stirring for 15 min, a solution containing 31.5 mg (0.15 mmol) of pentafluorobenzoic acid (C_6F_5COOH) in 0.5 mL of anhydrous THF was added dropwise. The resulting solution underwent a color change from blue to teal. The solution was stirred for 30 min and then filtered using a 25 mm diameter, 0.2 μm hydrophobic polytetrafluoroethylene (PTFE) syringe filter into a separate dry 25 mL Schlenk flask to remove all molecular sieve particulate. The solvent was removed *in vacuo* and the resulting teal oil was triturated with pentane (3 x 5 mL) until a powdery teal solid was obtained. The product was further stirred in 10 mL anhydrous pentane overnight (12 h) and the solid was collected by filtration, washed with ~5 mL anhydrous pentane, dried on a vacuum line for ~ 6 h (98.6 mg, 66% yield). UV-vis (THF, 25˚C) λ_{max}, nm (ε, M^{-1} cm^{-1}): 375 (~3000), 598 (440). HR-MS (ESI, THF, negative ion) *m/z*: $[LCu^{II}(O_2CC_6F_5)]^-$ Calcd. for $[C_{38}H_{37}F_5CuN_3O_4]^-$ 757.2918; found 757.2027. Anal. Calc. for $C_{38}H_{37}F_5CuN_3O_4$: C, 64.81; H, 7.35; N, 5.60. Found: C, 65.36; H, 7.54; N, 5.43.

$[NBu_4][LCu^{II}(O_2CC_6H_2(iPr_3))]$. The same synthesis was followed for $[NBu_4][LCu^{II}(O_2CC_6H_2(iPr_3))]$ as reported above for the synthesis of $[NBu_4][LCu^{II}(O_2CC_6F_5)]$ with the following exceptions: a solution of 2,4,6-triisopropylbenzoic acid (36.9 mg, 0.15 mmol) in 0.5 mL dry THF was added in place of pentafluorobenzoic acid. Upon addition of the 2,4,6-triisopropylbenzoic acid, the solution immediately turned green. The same method was followed as for $[NBu_4][LCu^{II}(O_2CC_6F_5)]$ to isolate and dry $[NBu_4][LCu^{II}(O_2CC_6H_2(iPr_3))]$, resulting in a

fine green powder (81.4 mg, 53% yield). UV-vis (THF, 25 °C) λ_{max}, nm (ε, M^{-1} cm^{-1}): 673 (300). HR-MS (ESI, THF, negative ion) *m/z*: $[LCu^{II}(O_2CC_6H_2(iPr_3))]^-$ Calcd. for $[C_{47}H_{60}CuN_3O_4]^-$ 793.3866; found 793.3978. Anal. Calc. for $C_{47}H_{60}CuN_3O_4$: C, 71.43; H, 8.72; N, 6.06. Found: C, 70.73; H, 8.87; N, 5.63. For the purpose of obtaining crystals suitable for analysis by X-ray diffraction, $[NEt_4][LCu^{II}(O_2CC_6H_2(iPr_3))]$ was prepared via an analogous procedure using $[NEt_4][LCu^{II}(OH)]$ as the precursor. X-ray quality crystals (dichroic teal/violet blocks) were formed upon slow diffusion of anhydrous diethyl ether into a concentrated THF solution of $[NEt_4][LCu^{II}(O_2CC_6H_2(iPr_3))]$ (~35 mM) at room temperature.

$[NBu_4][LCu^{II}(O_2CC_6H_4(NO_2))]$. The same synthesis was followed as with the synthesis of $[NBu_4][LCu^{II}(O_2CC_6F_5)]$ with the following exceptions: 150 mg (0.19 mmol) of $[NBu_4][LCuOH]$ was added to THF over 3 Å sieves. Then, a solution of *p*-nitrobenzoic acid (31.1 mg, 0.19 mmol) in 0.5 mL THF was added in place of pentafluorobenzoic acid. The resulting teal green powder was isolated following the same method reported for $[NBu_4][LCu^{II}(O_2CC_6F_5)]$ in similar yield (103 mg, 58%). UV-vis (THF, 25˚C) λ_{max}, nm (ε, M^{-1} cm^{-1}): 365 (~2000), 600 (300). HR-MS (ESI, THF, negative ion) *m/z*: $[LCu^{II}(O_2CC_6H_4(NO_2))]^-$ Calcd. for $[C_{38}H_{41}CuN_4O_6]^-$ 712.2317; found 712.2884. Anal. Calc. for $C_{54}H_{77}CuN_5O_6$: C, 67.86; H, 8.12; N, 7.32. Found: C, 67.46; H, 8.05; N, 7.24.

$[NBu_4][LCu^{II}(O_2CC_6H_5)]$. The same synthesis was followed as with the synthesis of $[NBu_4][LCu^{II}(O_2CC_6F_5)]$ with the following exceptions: a solution of benzoic acid (18.2 mg, 0.15 mmol) in 0.5 mL THF was added in place of pentafluorobenzoic acid. The resulting teal blue powder was isolated following the same method reported for $[NBu_4][LCu^{II}(O_2CC_6F_5)]$ in similar yield (82.2 mg, 61% yield). UV-vis (THF, 25 ˚C) λ_{max}, nm (ε, M^{-1} cm^{-1}): 370 (~3300), 615 (420). HR-MS (ESI, THF, negative ion) *m/z*: $[LCu^{II}(O_2CC_6H_5)]^-$ Calcd. for $[C_{38}H_{42}CuN_3O_4]^-$ 667.2461; found 667.3313. Anal. Calc. for $C_{38}H_{42}CuN_3O_4$: C, 71.21; H, 8.63; N, 6.15. Found: C, 71.08; H, 8.65; N, 6.08.

$[NBu_4][LCu^{II}(O_2CC_6H_4(OMe))]$. The same synthesis was followed as for the synthesis of $[NBu_4][LCu^{II}(O_2CC_6F_5)]$ with the following exceptions: 150 mg (0.19 mmol) of $[NBu_4][LCuOH]$ was added to THF over 3 Å sieves. Then, a solution of *p*-methoxybenzoic acid (28.3 mg, 0.19 mmol) in 0.5 mL dry THF was added in place of pentafluorobenzoic acid. The resulting teal blue

powder was isolated following the same method reported for $[NBu_4][LCu^{II}(O_2CC_6F_5)]$ in similar yield (108.2 mg, 59% yield). UV-vis (THF, 25 °C) λ_{max}, nm (ε, M^{-1} cm^{-1}): 370 (~2500), 618 (400). HR-MS (ESI, THF, negative ion) *m/z*: $[LCu^{II}(O_2CC_6H_4(OMe))]^-$ Calcd. for $[C_{39}H_{44}CuN_3O_5]^-$ 697.2571; found 697.3812. Anal. Calc. for $C_{39}H_{44}CuN_3O_5$: C, 70.22; H, 8.57; N, 5.96. Found: C, 69.37; H, 8.44; N, 5.85.

$[NBu_4][LCu^{II}(O_2CCH_3)]$. The synthesis of $[NBu_4][LCu^{II}(O_2CCH_3)]$ was adapted from the previously published synthesis of $[NBu_4][LCu^{II}OH]$.[2] A 25 mL Schlenk flask in a nitrogen filled glovebox at room temperature was charged with 100 mg (0.17 mmol) of solid $LCu^{II}(MeCN)$. To this flask, ~10 mL of anhydrous diethyl ether was added, resulting in a red-brown slurry. After stirring for 15 min, a solution containing 48.7 mg (0.16 mmol) of tetrabutylammonium acetate, $(NBu_4)(O_2CCH_3)$, in 0.5 mL of anhydrous THF was added dropwise. Upon addition of the THF solution, a teal blue solid precipitated out immediately. The mixture was stirred for 30 min, solvent was removed *in vacuo* and the resulting teal oil was triturated with pentane (3 x 5 mL) until a powdery teal solid was obtained. The product was further stirred in 10 mL anhydrous pentane overnight (12 h) and the solid was collected by filtration, washed with ~5 mL anhydrous pentane and dried on a vacuum line for ~ 6 h (107.9 mg, 79% yield). UV-vis (THF, 25˚C) λ_{max}, nm (ε, M^{-1} cm^{-1}): 370 (~2500), 619 (350). HR-MS (ESI, THF, negative ion) *m/z*: $[LCu^{II}(O_2CCH_3)]^-$ Calcd. for $[C_{33}H_{40}CuN_3O_4]^-$ 605.2329; found 605.2491. Anal. Calc. for $C_{33}H_{40}CuN_3O_4$: C, 69.34; H, 9.03; N, 6.60. Found: C, 69.20; H, 9.12; N, 6.16. X-ray quality crystals (dichroic blue/violet blocks) were formed upon slow diffusion of anhydrous diethyl ether into a concentrated THF solution of $[NBu_4][LCu^{II}(O_2CCH_3)]$ (~35 mM) at room temperature.

2. General procedure for the generation of $[Cu(O_2CR)]^{2+}$ species.

A necked 1 cm UV-vis cuvette in the Unisoku low temperature UV-vis cell holder containing 1.9 mL of dry THF or 1,2-DFB and a stir bar was cooled to –80 °C or –25 °C, respectively. To a given cell, 0.05 mL of 8 mM solution of complex (for 0.2 mM final Cu concentration) or 0.05 mL of 4 mM of complex (for 0.2 mM final Cu concentration) was added. After mixing and allowing for temperature stabilization (1 min), a UV-vis spectrum was recorded. To the stirring mixture, 0.05 mL of 8 mM $[AcFc][BAr^F{}_4]$ (for 0.2 mM final concentration) or 4 mM $[AcFc][BAr^F{}_4]$ (for 0.1 mM final concentration) was injected, stirred and a spectrum immediately recorded.

3. General procedure for the reversible oxidation/reduction of $[NBu_4][LCu^{II}O_2CR]$.

To two cuvettes each with 1.65 mL THF and a stir bar in a Unisoku low temperature cell holder at –80 °C was added 0.05 mL of a stock solution of $[NBu_4][LCu^{II}(O_2CC_6H_4(NO_2))]$ and $[NBu_4][LCu^{II}(O_2CC_6H_4(OMe))]$, respectively (8 mM). After temperature equilibration (5 min), 0.05 mL of the 8 mM THF solution of $[AcFc][BAr^F{}_4]$ was injected into each cuvette, stirred and the spectrum immediately recorded. To this oxidized solution, 0.05 mL of 8 mM decamethylferrocene (Fc*) in THF was added and the resulting spectrum recorded. The addition of 0.05 mL of $[AcFc][BAr^F{}_4]$ (oxidant) and 0.05 mL Fc* (reductant) was repeated with spectra taken after each addition a total of three times.

4. General procedure for kinetics analysis of the reactions of $[LCu^{III}(O_2CR)]$ with TTBP.

A necked 1 cm UV-vis cuvette in the Unisoku low temperature UV-vis cell holder containing 1.85 mL THF was cooled to –80 °C. To this cell 0.05 mL of 8 mM THF solution of complex (for 0.2 mM final Cu concentration) or 0.05 mL 4 mM THF solution of complex (for 0.1 mM final Cu concentration) was added. Continuous collection of the UV-vis absorption spectrum was initiated as soon as 0.05 mL of 8 mM $[AcFc][BAr^F{}_4]$ for 0.2 mM final concentration (or 4 mM for 0.1 mM final concentration) was injected into the cuvette. Upon observation of the full growth of the oxidized feature of $LCu^{III}(O_2CC_6F_5)$, $LCu^{III}(O_2CC_6H_4(NO_2))$, $LCu^{III}(O_2CC_6H_4(OMe))$, $LCu^{III}(O_2CC_6H_5)$ or $LCu^{III}(O_2CCH_3)$, 0.05 mL of a solution of TTBP (50 equiv) was added to the cell and the spectrum monitored until changes ceased. The resulting kinetics data were fit to a second order reaction model using global fitting software, ReactLab KINETICS.

5. General procedure for kinetics analysis of the reactions of $[LCu^{III}(O_2CR)]$ with DHA.

The same procedure was followed for reactions of $[LCu^{III}(O_2CR)]$ with DHA as detailed in the above section with the following exceptions: (i) 1,2-DFB was used as a solvent in place of THF which was cooled to –25 °C instead of –80 °C and (ii) 200 equiv excess of DHA were used.

6. Procedure for kinetics analysis of the reaction of $[LCu^{III}(O_2CC_6H_4(m\text{-}Cl))]$ with 1,4-CHD.

A reaction between $LCu^{III}(O_2CC_6H_4(m\text{-}Cl))$ and 200 eq. of CHD was performed by cooling a UV-vis cuvette under Ar and containing a stir bar and DFB (1.8 mL) to –25 °C. A solution of $[NBu_4][LCu(O_2CC_6H_4(m\text{-}Cl))]$ in DFB (0.05 mL, 8 mM) was added to the cuvette. An aliquot of $[AcFc][BAr^F{}_4]$ in DFB (0.05 mL, 8 mM) was injected into the cuvette. Continuous collection of the UV-vis spectrum was initiated as soon as a CHD solution in DFB (0.1 mL, 800 mM) was added to the cuvette. The collection of the spectra continued until full decay of the signal from $LCu(O_2CC_6H_4(m\text{-}Cl))$ was observed. The experiment was repeated two more times under the same conditions. The kinetics obtained from this reaction were analyzed by a global analysis (350-850 nm) of the data using ReactLab Kinetics. The average k_2 value was calculated to be 4.6×10^{-2} M^{-1} s^{-1}.

7. X-Ray crystallographic information.

Table S1. Selected bond distances (Å) and angles (°) from the X-Ray crystal structures of $[NEt_4][LCu(O_2CC_6H_4(Cl))]$, $[NEt_4][LCu(O_2CC_6H_2(iPr_3))]$ and $[NBu_4][LCu(O_2CCH_3)]$.

	$[NEt_4]$ $[\mathbf{LCu^{II}(O_2CC_6H_4(Cl))}]$	$[NEt_4]$ $[\mathbf{LCu^{II}(O_2CC_6H_2(iPr_3))}]$	$[NBu_4]$ $[\mathbf{LCu^{II}(O_2CCH_3)}]$
Cu – O1, Å	1.929(3)	1.9055(12)	1.9452(17)
Cu – O2, Å	2.516(3)	2.9190(14)	2.5450(19)
Cu – N1, Å	2.005(3)	1.9906(13)	2.0158(18)
Cu – N2, Å	1.912(3)	1.9148(14)	1.9400(18)
Cu – N3, Å	2.018(3)	–	2.0163(19)
Cu – O4, Å	–	2.0020(12)	–
N3 – C17, Å	–	1.290(2)	–
O4 – C17, Å	–	1.3049(18)	–
N1 – C23, Å	–	1.347(2)	–
O3 – C23, Å	–	1.2470(19)	–
N1 – Cu – N3, °	160.44(13)	–	159.59(7)
N1 – Cu – O4, °	–	162.12(5)	–
N1 – Cu – N2, °	80.48(12)	81.06(6)	80.44(8)
N2 – Cu – O1, °	176.17(12)	170.92(6)	172.50(8)
τ_4	0.19	0.19	0.20

8. UV-Vis spectra overlay.

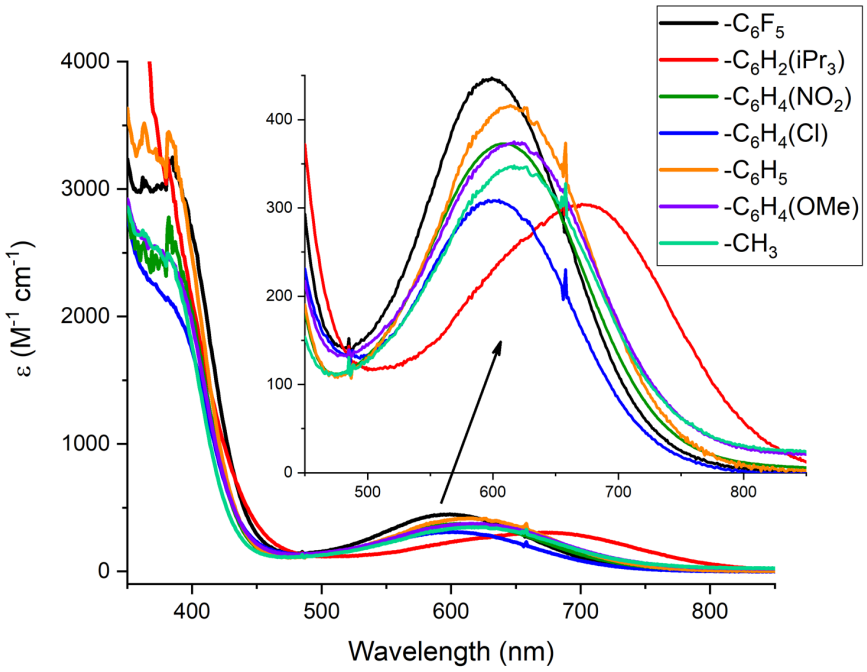

Figure S1. UV-vis spectra overlay of [NBu_4][$LCu^{II}(O_2CR)$] where R = $–C_6H_4(Cl)$ (blue), $–C_6F_5$ (black), $–C_6H_2(iPr_3)$ (red), $–C_6H_4(NO_2)$ (green), $–C_6H_5$ (orange), $–C_6H_4(OMe)$ (violet) and $–CH_3$ (light green) in THF at 25 °C. NOTE: The spectrum corresponding to R = $–C_6H_2(iPr_3)$ (red) is a clear outlier in comparison to the other complexes under the same conditions; this is attributed to the *N,N',O*-coordination observed for R = $–C_6H_2(iPr_3)$.

9. EPR spectral data.

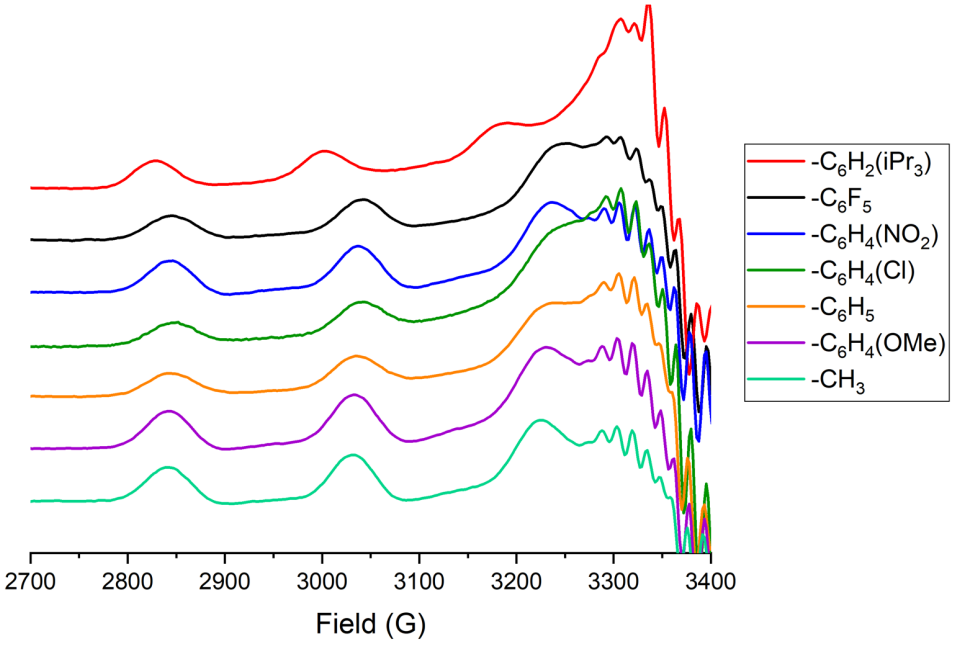

Figure S2. Overlay of continuous X-band (9.64 GHz) EPR spectra with zoomed view of copper hyperfine structure of [NBu$_4$][LCu^{II}(O$_2$C–R)] where R = –C$_6$H$_2$(iPr$_3$) (red), –C$_6$F$_5$ (black), –C$_6$H$_4$(NO$_2$) (blue), –C$_6$H$_4$(Cl) (green), –C$_6$H$_5$ (orange), –C$_6$H$_4$(OMe) (violet) and –CH$_3$ (light green) in THF at 30 K.

Table S2. Simulated g-values and hyperfine/superhyperfine parameters (MHz) for Cu, N^{amide} and N^{pyridine} nuclei for [NBu$_4$][LCu^{II}(O$_2$C–**R**)] complexes in THF at 30 K.

R =	**–C$_6$H$_4$(Cl)**	**–C$_6$H$_2$(iPr$_3$)**	**–C$_6$F$_5$**	**–C$_6$H$_4$(NO$_2$)**	**–C$_6$H$_5$**	**–C$_6$H$_4$(OMe)**	**–CH$_3$**
g_x	2.035	2.060	2.028	2.030	2.0350	2.035	2.030
g_y	2.048	2.040	2.055	2.045	2.0480	2.055	2.050
g_z	2.200	2.228	2.197	2.202	2.2000	2.205	2.204
$A^{Cu}{}_x$	55	30	60	60	60	40	60
$A^{Cu}{}_y$	60	50	60	60	60	55	60
$A^{Cu}{}_z$	575	545	580	575	575	575	573
$A^{py}{}_x$	30	30	30	30	30	30	30
$A^{py}{}_y$	45	40	45	45	45	50	45
$A^{py}{}_z$	47	50	55	35	47	35	30
$A^{am}{}_x$	40	30	30	45	45	45	45
$A^{am}{}_y$	50	40	45	50	50	50	50
$A^{am}{}_z$	55	50	55	35	55	35	30

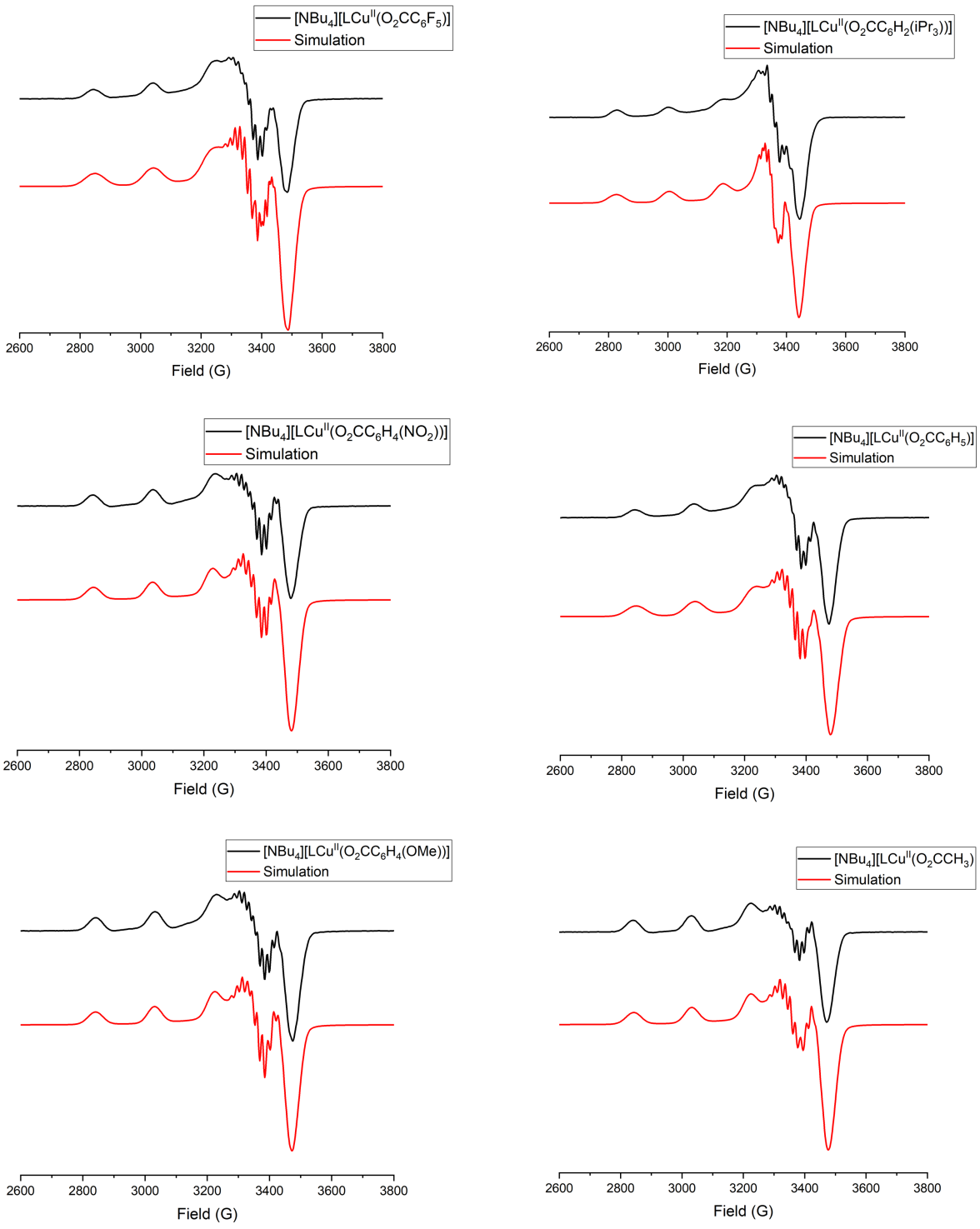

Figure S3. Overlay of experimental (black) and simulated (red) continuous wave X-band (9.64 GHz) EPR spectra of [NBu4][LCu^{II}(O$_2$C–R)]; R = –C$_6$F$_5$ (top left), –C$_6$H$_2$(iPr$_3$) (top right), –C$_6$H$_4$(NO$_2$) (middle left), –C$_6$H$_5$ (middle right), –C$_6$H$_4$(OMe) (bottom left) and –CH$_3$ (bottom right) in THF at 30 K.

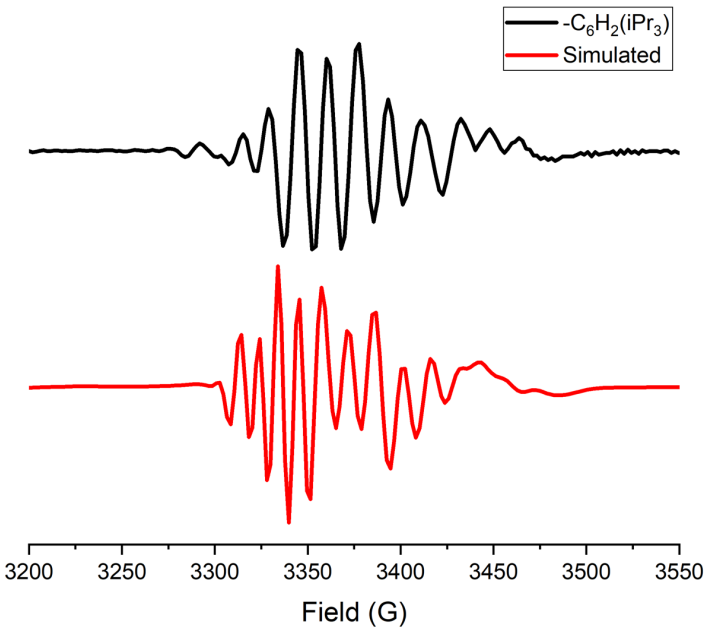

Figure S4. Overlay of the experimental (black) and simulated (red) second derivative of the continuous wave X-band (9.64 GHz) EPR spectrum of $[NBu_4][LCu^{II}(O_2CC_6H_2(iPr_3))]$.

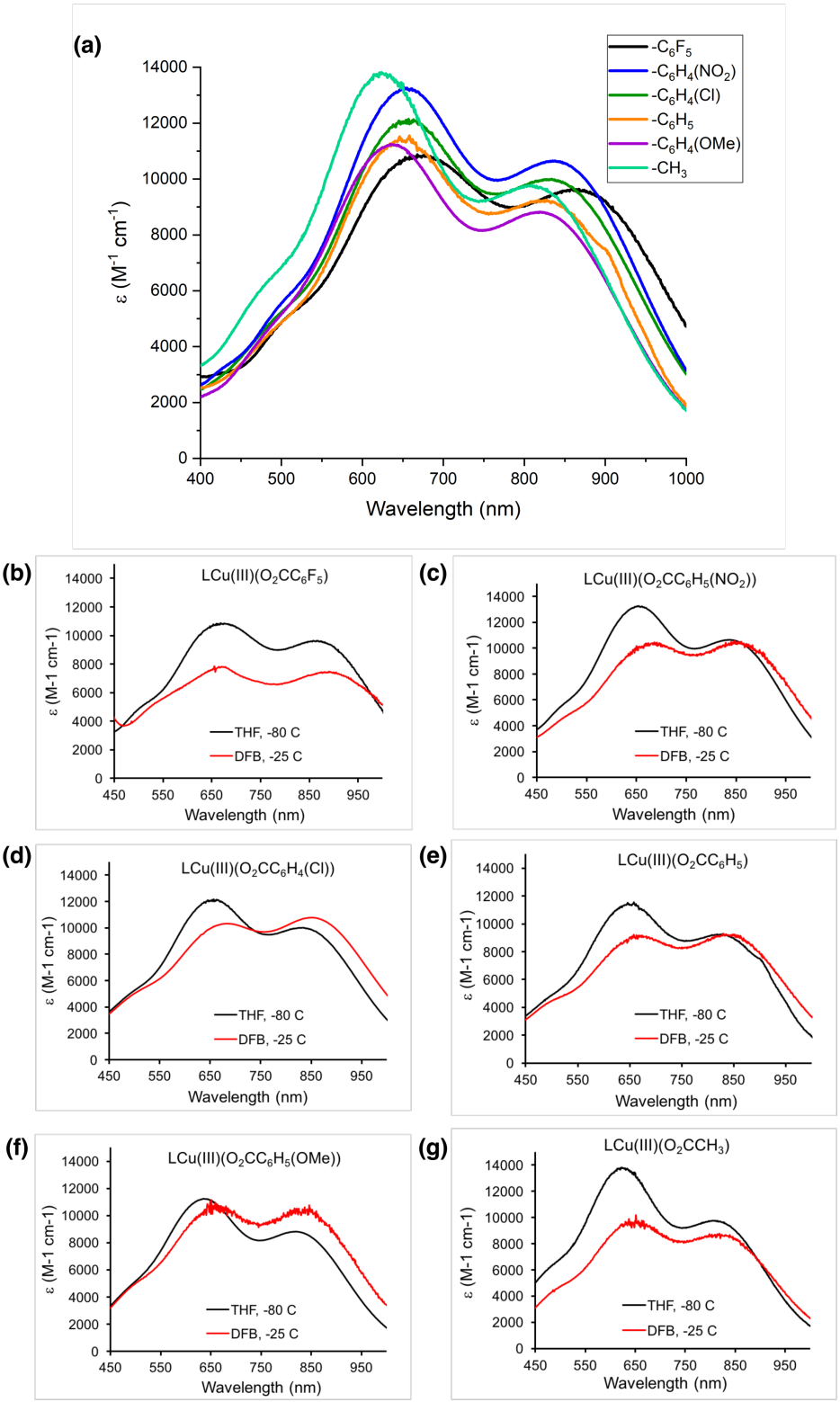

Figure S5. (a) UV-vis spectra overlay of $LCu^{III}(O_2CR)$ where R = $–C_6F_5$ (black), $–C_6H_4(NO_2)$ (blue),–$C_6H_4(Cl)$ (green), $–C_6H_5$ (orange), $–C_6H_4(OMe)$ (violet) and $–CH_3$ (light green) in THF at –80 °C. (b) – (g) overlay of data for each LCu^{III} complex under two conditions (black = THF at –80 °C, red = DFB at –25°C).

10. Individual cyclic voltammograms.

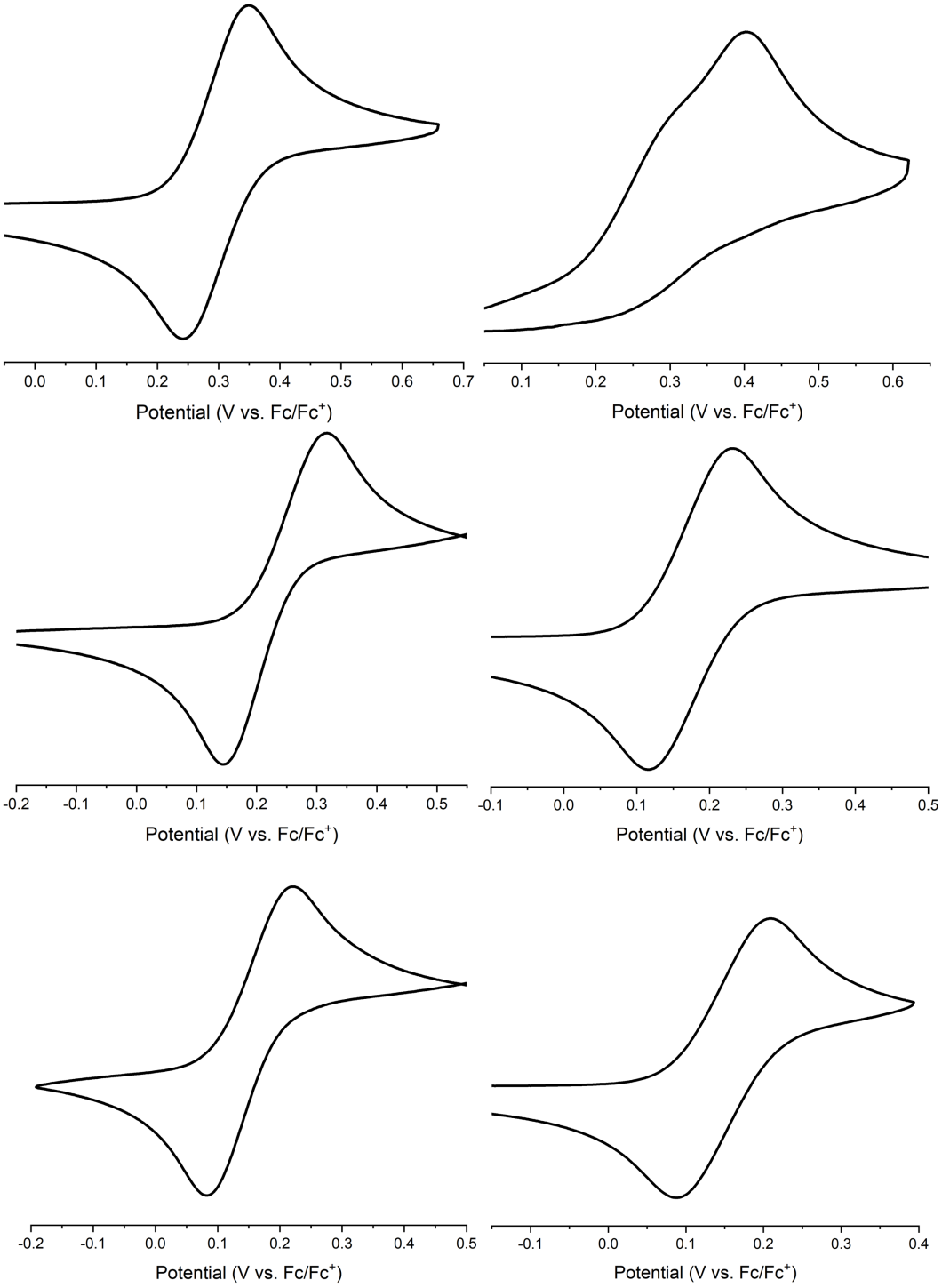

Figure S6. Individual cyclic voltammograms collected of $[NBu_4][LCu^{II}(O_2C–R)]$; R = $–C_6F_5$ (top left), $–C_6H_2(iPr_3)$ (top right), $–C_6H_4(NO_2)$ (middle left), $–C_6H_5$ (middle right), $–C_6H_4(OMe)$ (bottom left) and $–CH_3$ (bottom right); 2 mM LCu^{II}/0.3 M TBAP in THF, 25 °C, glassy carbon working electrode, 100 mV/s scan rate.

11. Monitoring the oxidation of Cu^{II} to Cu^{III} via UV-Vis.

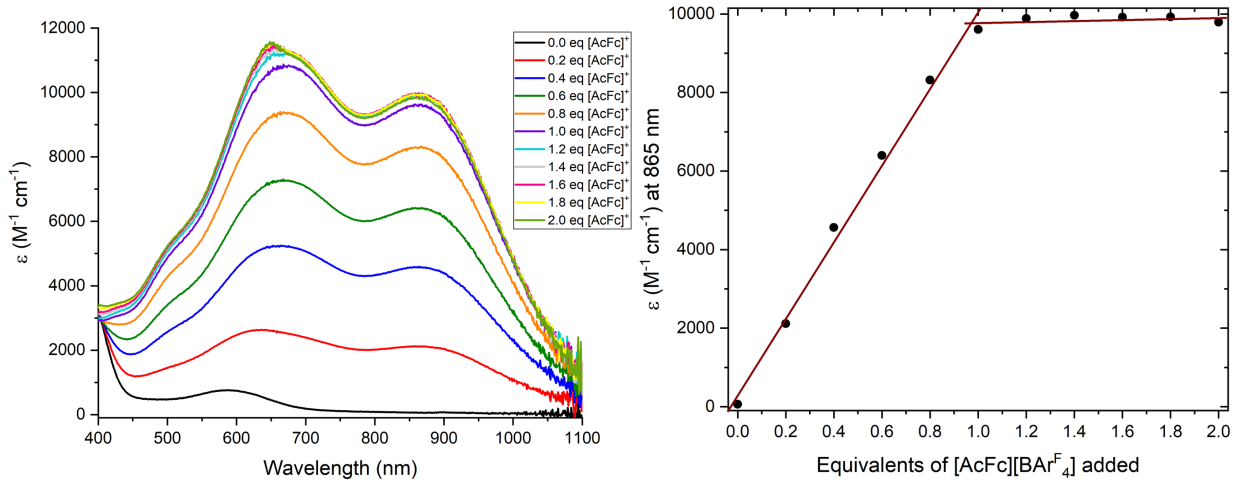

Figure S7. (left) Overlay of UV-vis spectra upon addition of varying equivalents of $[AcFc][BAr^F{}_4]$ to $[NBu_4][LCu^{II}(O_2CC_6F_5)]$ at –80 °C in THF; (right) plot of corresponding molar absorptivity values at λ = 865 nm vs. equivalents of $[AcFc][BAr^F{}_4]$.

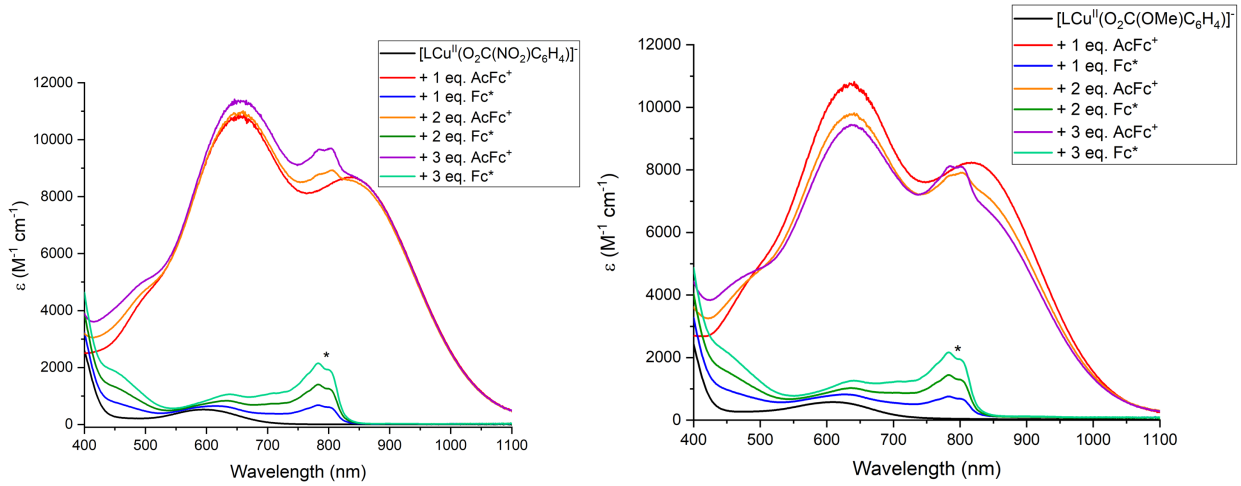

Figure S8. UV-vis oxidation/reduction titration where 1–3 equivalents of $[AcFc][BAr^F{}_4]$ and decamethyl ferrocene (Fc*) were added to (left) $[NBu_4][LCu^{II}(O_2CC_6H_4(NO_2))]$ and (right) $[NBu_4][LCu^{II}(O_2CC_6H_4(OMe))]$ in THF at –80 °C (*denotes decamethyl ferrocenium signal).

12. UV-vis spectra decay traces during reaction.

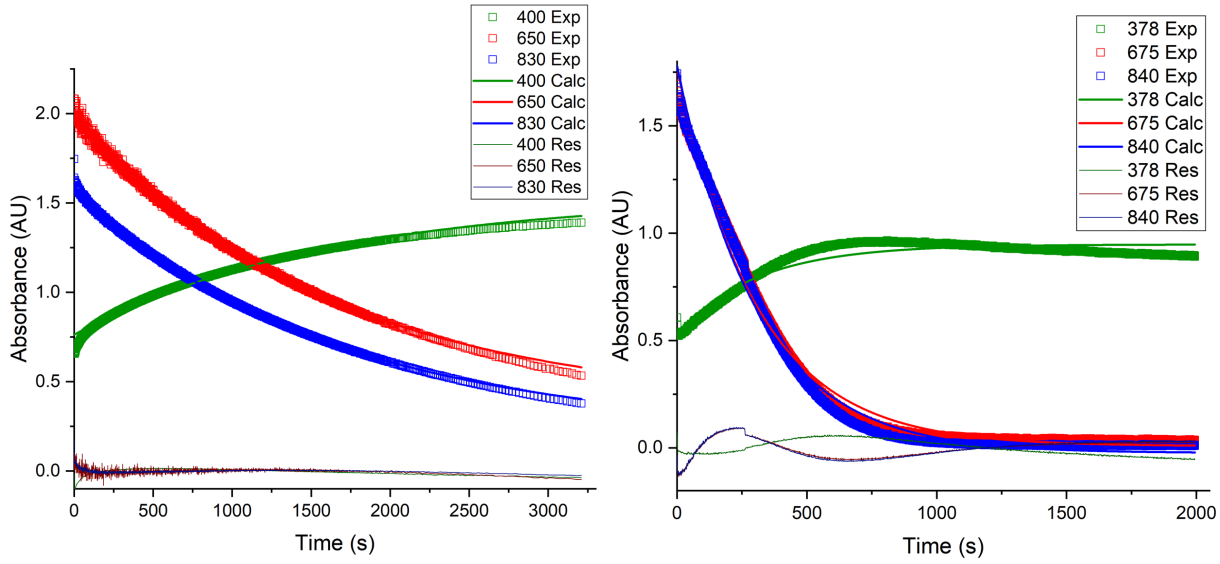

Figure S9. Representative UV-vis spectra decay traces of $LCu^{III}(O_2CC_6H_5)$ with (left) 50 eq. TTBP in THF at –80 °C and (right) 200 eq. DHA in 1,2-DFB at –25 °C; experimental decay traces at 400/378, 650/675 and 830/840 nm (green, red and blue squares, respectively) overlaid with calculated decay traces at 400/378, 650/675 and 830/840 nm (green, red, and blue lines, respectively) and calculated residuals from kinetic fits at 400/378, 650/675 and 830/840 nm (dark green, dark red, and dark blue lines, respectively). The decay traces shown have not been normalized for concentration (0.2 mM Cu^{III}), however, kinetic fits of triplicate runs in ReactLab KINETICS were made with consideration of concentration.

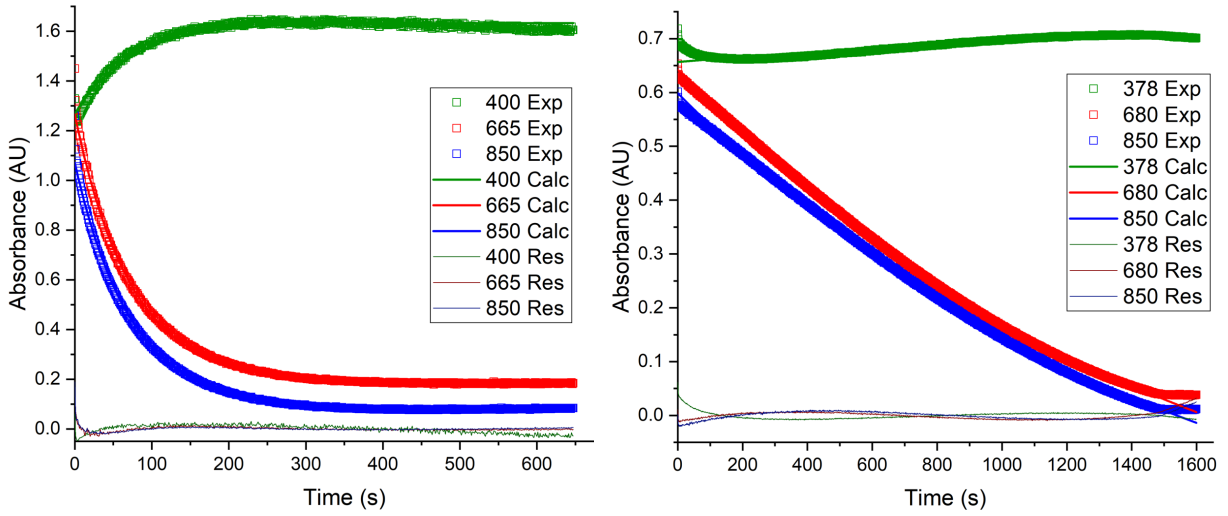

Figure S10. Representative UV-vis spectra decay traces of $LCu^{III}(O_2CC_6F_5)$ with (left) 50 eq. TTBP in THF at –80 °C and (right) 200 eq. DHA in 1,2-DFB at –25 °C; experimental decay traces at 400/378, 665/680 and 850 nm (green, red and blue squares, respectively) overlaid with calculated decay traces

at 400/378, 665/680 and 850 nm (green, red, and blue lines, respectively) and calculated residuals from kinetic fits at 400/378, 665/680 and 850 nm (dark green, dark red, and dark blue lines, respectively). The decay traces shown have not been normalized for concentration (0.2 mM Cu^{III}), however, kinetic fits of triplicate runs in ReactLab KINETICS were made with consideration of concentration.

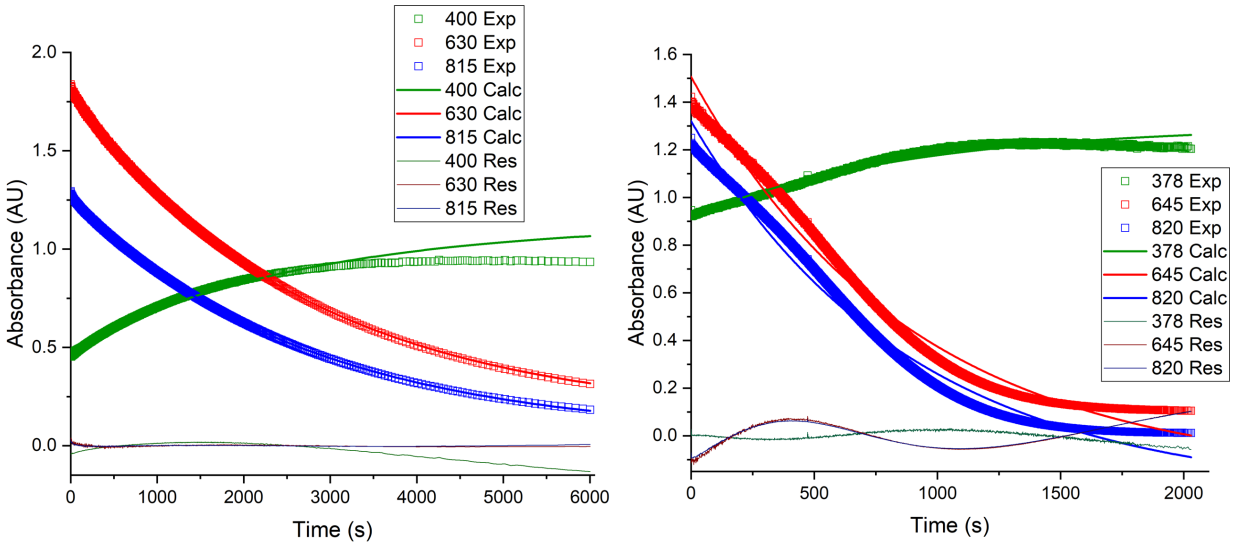

Figure S11. Representative UV-vis spectra decay traces of $LCu^{III}(O_2CCH_3)$ with (left) 50 eq. TTBP in THF at –80 °C and (right) 200 eq. DHA in 1,2-DFB at –25 °C; experimental decay traces at 400/378, 630/645 and 815/820 nm (green, red and blue squares, respectively) overlaid with calculated decay traces at 400/378, 630/645 and 815/820 nm (green, red, and blue lines, respectively) and calculated residuals from kinetic fits at 400/378, 630/645 and 815/820 nm (dark green, dark red, and dark blue lines, respectively). The decay traces shown have not been normalized for concentration (0.2 mM Cu^{III}), however, kinetic fits of triplicate runs in ReactLab KINETICS were made with consideration of concentration.

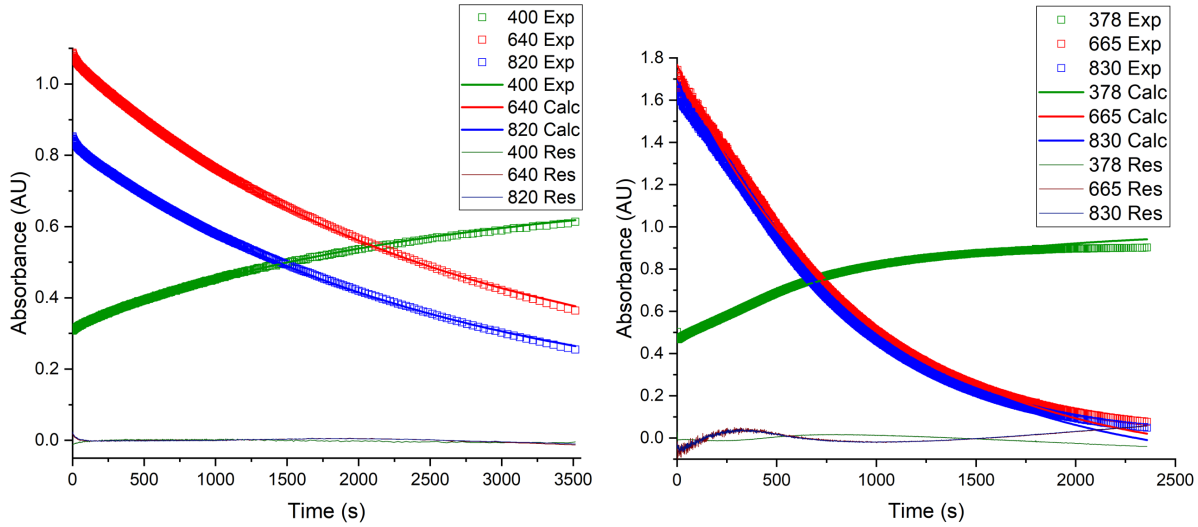

Figure S12. Representative UV-vis spectra decay traces of $LCu^{III}(O_2CC_6H_4(OMe))$ with (left) 50 eq. TTBP in THF at –80 °C and (right) 200 eq. DHA in 1,2-DFB at –25 °C; experimental decay traces at

400/378, 650/675 and 820/830 nm (green, red and blue squares, respectively) overlaid with calculated decay traces at 400/378, 650/675 and 820/830 nm (green, red, and blue lines, respectively) and calculated residuals from kinetic fits at 400/378, 650/675 and 820/830 nm (dark green, dark red, and dark blue lines, respectively). The decay traces shown have not been normalized for concentration (0.1 mM Cu^{III} with TTBP and 0.2 mM Cu^{III} with DHA), however, kinetic fits of triplicate runs in ReactLab KINETICS were made with consideration of concentration.

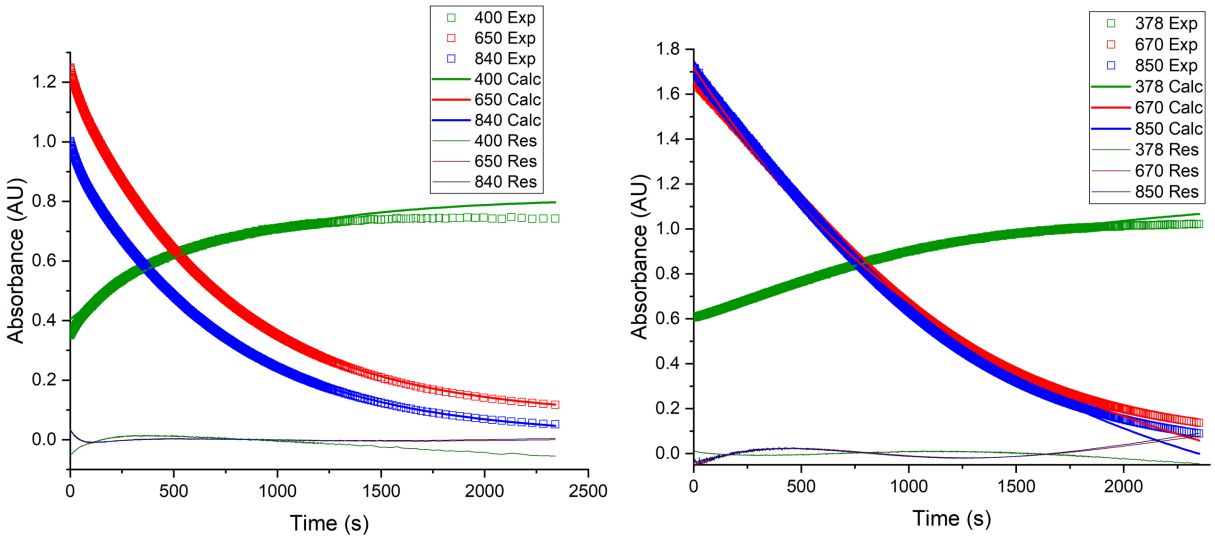

Figure S13. Representative UV-vis spectra decay traces of $LCu^{III}(O_2CC_6H_4(NO_2))$ with (left) 50 eq. TTBP in THF at –80 °C and (right) 200 eq. DHA in 1,2-DFB at –25 °C; experimental decay traces at 400/378, 650/670 and 840/850 nm (green, red and blue squares, respectively) overlaid with calculated decay traces at 400/378, 650/670 and 840/850 nm (green, red, and blue lines, respectively) and calculated residuals from kinetic fits at 400/378, 650/670 and 840/850 nm (dark green, dark red, and dark blue lines, respectively). The decay traces shown have not been normalized for concentration (0.1 mM Cu^{III} with TTBP and 0.2 mM Cu^{III} with DHA), however, kinetic fits of triplicate runs in ReactLab KINETICS were made with consideration of concentration.

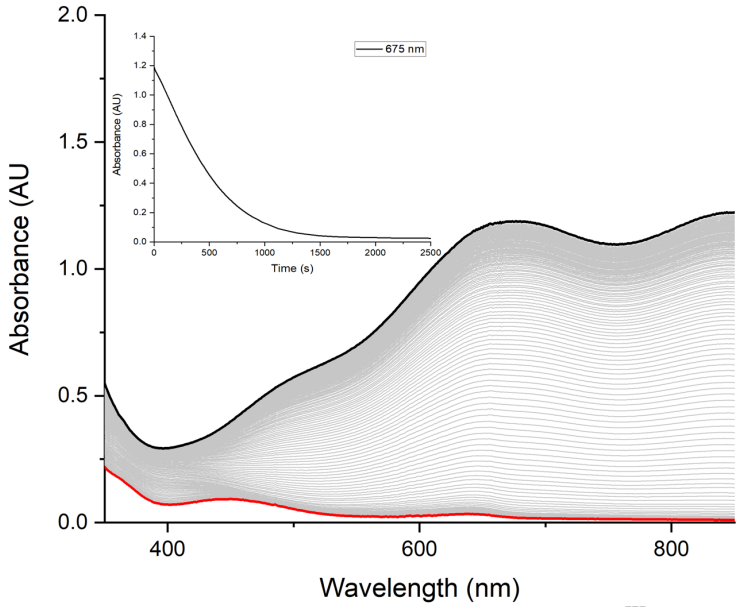

Figure S14. Overlay of the UV-vis spectra for the reaction of $LCu^{III}(O_2CC_6H_4(m\text{-}Cl))$ with 200 eq. of CHD in DFB at –25 °C (inset: UV-vis decay trace at 675 nm).

13. Reactivity plot ($\log k_2$) for $[LCu^{III}O_2CR]$/TTBP pair.

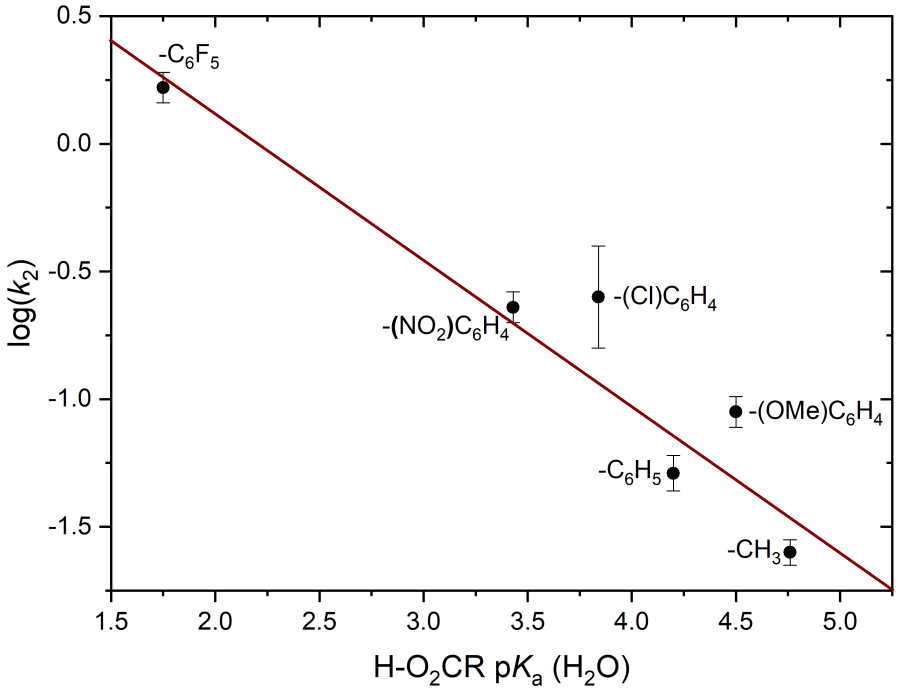

Figure S15. Plot of $\log k_2$ for the reaction of $[LCu^{III}O_2CR]$ with TTBP (THF) at –80 °C vs. HO_2C–R pK_a (H_2O). Dark red line is linear fit to $\log(k_2) = -0.57pK_a + 1.2$, $R^2 = 0.93$.

Table S3. O–H BDE values for HO_2C-R carboxylic acids.

*HO_2C–**R***	*O–H BDE (kcal mol^{-1})*
–C_6F_5	–
–$C_6H_2(iPr_3)$	–
–$C_6H_4(NO_2)$	~ 107.1[7]
–$C_6H_4(Cl)$	~ 107.3[7]
–C_6H_5	111.0 ± 4.0[8]
–$C_6H_4(OMe)$	~ 106.8[7]
–CH_3	112.0 ± 3.0[8]

14. Computation protocol.

Geometry optimizations and frequency calculations are done at the density functional theory (DFT) level using Gaussian 09 and Gaussian 16 electronic structure packages.[9] Geometry optimizations are done in the gas-phase at B3LYP-D3(BJ)/basis-I level of theory,[10,11] (*basis-I*: 6-31G(d) basis set[12] for light atoms and the Stuttgart/Dresden effective core potential with its associated basis set (SDD)[13] for Cu). An "ultrafine" grid was used for numerical integration in DFT, along with an integral accuracy set at 10^{-12}. Natures of all stationary points are verified by calculation of quasi-harmonic vibrational frequencies at the same level of theory, while replacing low frequency vibrational modes (below 50 cm^{-1}) with a value of 50 cm^{-1}. Electronic energies were further refined by performing single point calculations using the def2-TZVP basis set[14] for non-metals and SDD for Cu (*basis-II*). Solvent reaction field similar to experiment was introduced employing the SMD continuum solvation model[15] using solvent parameters for tetrahydrofuran (THF, ε = 7.4). All transition-state (TS) structures were located on the broken-symmetry (BS) singlet surface, and the final electronic energies were spin-purified using the approximate spin-projection scheme proposed by Yamaguchi et al.[16] Experimental UV-Vis spectral features were modeled using time-dependent density functional theory (TD-DFT) calculations at the PBE0-D3(BJ)/basis-III level[17] using B3LYP-D3(BJ)/basis-I geometries. (*basis-III*: def2-TZVP basis for non-metals and the def2-TZVPP basis and SDD pseudo-potential for Cu).

15. Cartesian coordinates of structures.

Cartesian coordinates of all optimized structures can be accessed from the coordinate file (.xyz).

16. Computed UV-Vis spectra.

In order to characterize the experimentally observed UV-Vis spectral features of various $LCu^{III}(O_2CR)$ species, TD-DFT calculations were carried out on all the complexes at the PBE0-D3(BJ)/basis-III/SMD(THF) level of theory on B3LYP-D3(BJ)/basis-I optimized geometries. As discussed in greater detail in the sister article,[6] TD-DFT calculations suggest that the intense UV-vis transitions of the copper-complex with R = -C_6H_4(*m*-Cl) at λ_{max} = 650 and 830 nm are attributable to varying compositions of two different ligand-to-metal charge-transfer (LMCT) transitions involving the supporting ligand (L^{2-}) and the copper center: (1) N-aryl π → Cu $d_{x^2-y^2}$ and (2) N-amide π → Cu $d_{x^2-y^2}$. The nature of this transition is retained with electronic perturbation of the ligand framework, although there are small variations in energetics. As shown in Table S4, the two lowest energy transitions, i.e., those peaks centered from ~1.5-1.6 eV and from 1.9-2.0 eV, arise due to promotions of electrons from occupied aryl π and amide π orbitals of the dicarboxamido ligand to the lowest unoccupied molecular orbital—a vacant Cu $d_{x^2-y^2}$ orbital (e.g. combinations of HOMO-4 and HOMO → LUMO, Figure S15). Higher-energy peaks centered from ~2.5-2.6 eV arise in all cases as transitions from the carboxylate ligand to the LUMO. For the all substituted benzoate species (except for R = –CH_3), transition occurs primarily from the aryl π (e.g., HOMO-7, Figure S15) region of the benzoate groups. For the complex with R = –CH_3, however, no aryl π moiety is present, and it is the π-density of the acetate functionality (C=O) that is involved, leading to a significant shift in peak position compared to the aryl cases.

While Table S4 indicates that theory computes transition energies within 0.2 eV of experiment, which is a typical error bar for TD-DFT, there is only a modest correlation between theory and experiment for the variations of peak positions with substituents. As these variations over the entire series are already themselves only 0.1 to 0.2 eV, this is a difficult trend to fully capture, especially within the context of a linear response formalism for solvatochromic effects.[18] Nevertheless, the qualitative character of the various transitions is clearly secure.

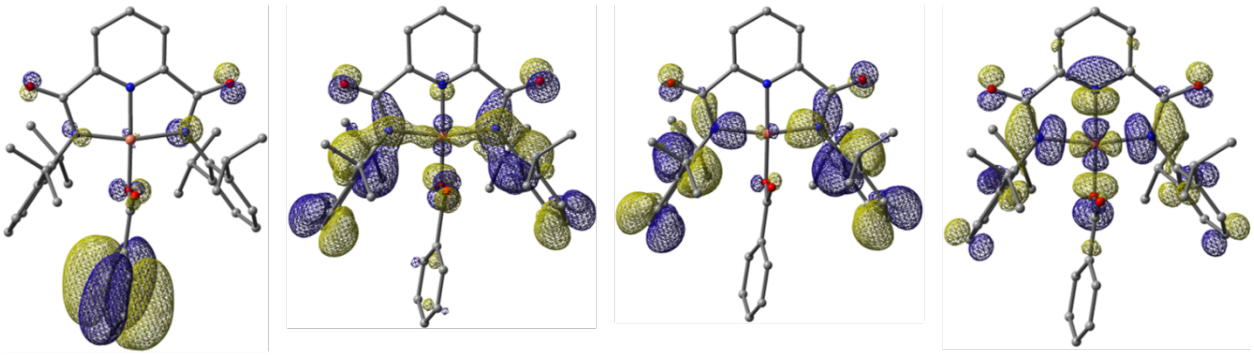

Figure S16. Highest occupied molecular orbital (HOMO), HOMO-7 and HOMO-4, together with the lowest unoccupied molecular orbital (LUMO) for complex **LCu^{III}O$_2$CC$_6$H$_5$**. H-atoms omitted for clarity.

Table S4. Computed excitation energies (eV; with experimental values in parentheses) for the different copper(III)-carboxylates obtained at PBE0-D3(BJ)/basis-III/SMD(THF)//B3LYP-D3(BJ)/basis-I level of theory.

Species	Excitation energy (eV)		
	Feature-I	Feature-II	Feature-III
-C$_6$F$_5$	1.59 (1.43)	1.95 (1.85)	2.63 (2.45)
-C$_6$H$_4$(*p*-NO$_2$)	1.58 (1.48)	1.96 (1.90)	2.61 (2.50)
-C$_6$H$_4$(*m*-Cl)	1.63 (1.49)	1.90 (1.91)	2.65 (2.53)
-C$_6$H$_5$	1.61 (1.50)	1.97 (1.92)	2.54 (2.51)
-C$_6$H$_4$(*p*-OMe)	1.62 (1.50)	1.98 (1.95)	2.57 (2.56)
-CH$_3$	1.62 (1.53)	1.97 (1.99)	2.67 (2.65)

17. HOMO-LUMO energies of various Cu(III) carboxylates.

Variation in orbital energies of the highest occupied molecular orbital (HOMO) and the lowest unoccupied molecular orbital (LUMO) as a function of carboxylate acceptor ligand is presented in Table S5.

Table S5. Computed orbital energies of the HOMO and the LUMO for the different Cu(III)-carboxylate complexes obtained at PBE0-D3(BJ)/basis-III/SMD(THF)//B3LYP-D3(BJ)/basis-I level of theory.

Species	Energy (eV)		
	HOMO	**LUMO**	**HOMO-LUMO Gap**

-C_6F_5	-6.45	-4.04	2.40
-C_6H_4(*p*-NO_2)	-6.45	-4.04	2.41
-C_6H_4(*m*-Cl)	-6.42	-3.99	2.43
-C_6H_5	-6.39	-3.95	2.44
-C_6H_4(*p*-OMe)	-6.37	-3.92	2.45
-CH_3	-6.41	-3.94	2.47

18. Energetics for reactivity with Ar^2OH and DHA.

Single point electronic energies, E(sol), incorporating THF (ε = 7.4) solvation effects in the case of reactions with 2,6-di-*tert*-butyl-phenol (Ar^2OH) and that for cyclopentanone (ε = 13.6) in the case of 9,10-dihydroanthracene (DHA), spin-projected electronic energies for broken-symmetry singlet TS structures, E'(sol), and the absolute solution-phase Gibbs free energies, G(sol) of complexes with various carboxylate groups and corresponding TS structures with Ar^2OH and DHA are presented in Table S6. All energies are reported in Hartree.

Table S6. Solution phase electronic energies, E(sol)/Hartree, spin-projected electronic energies, E'(sol)/Hartree and the absolute solution-phase Gibbs free energies, G(sol)/Hartree for stationary points involving reaction of the mentioned Cu(III) benzoates with Ar^2OH and DHA computed at B3LYP/basis-II/SMD(sol)//B3LYP/basis-I level of theory.

File Description	**E(sol)/a.u.**	**E'(sol)/a.u. (Spin-purified)**	**G(sol)/a.u.**
Substrate-Ar2OH	-622.2877077		-621.9766137
Cu(III)-OOC-C6F5-Catalyst	-2633.303605		-2632.652231
Cu(III)-OOC-C6F5-Ar2OH-TS	-3255.597316	-3255.597323	-3254.625097
Cu(III)-OOC-C6H4(NO2)-Catalyst	-2341.541474		-2340.846779
Cu(III)-OOC-C6H4(NO2)-Ar2OH-TS	-2963.833387	-2963.83392	-2962.817448
Cu(III)-OOC-C6H4(Cl)-Catalyst	-2596.573596		-2595.890016
Cu(III)-OOC-C6H4(Cl)-Ar2OH-TS	-3218.866585	-3218.866594	-3217.861933
Cu(III)-OOC-C6H5-Catalyst	-2136.943133		-2136.249575
Cu(III)-OOC-C6H5-Ar2OH-TS	-2759.228065	-2759.228271	-2758.213523
Cu(III)-OOC-C6H4(OMe)-Catalyst	-2251.523581		-2250.798156
Cu(III)-OOC-C6H4(OMe)-Ar2OH-TS	-2873.809383	-2873.809803	-2872.763238
Substrate-DHA	-541.0004667		-540.8084917

Cu(III)-OOC-C6F5-DHA-TS	-3174.293383	-3174.293798	-3173.456992
Cu(III)-OOC-C6H4(NO2)-DHA-TS	-2882.529453	-2882.529503	-2881.648948
Cu(III)-OOC-C6H4(Cl)-DHA-TS	-3137.563799	-3137.563828	-3136.694417
Cu(III)-OOC-C6H5-DHA-TS	-2677.930776	-2677.930776	-2677.050927
Cu(III)-OOC-C6H4(OMe)-DHA-TS	-2792.512331	-2792.51231	-2791.601261

Table S7. Computed Gibbs free energies of activation, $\Delta G^{\ddagger}$ (kcal/mol) for the reactions of [$LCu^{III}O_2CR$] with DHA.[a]

R	$\Delta G^{\ddagger}$ [b]
C_6F_5	14.7
$C_6H_4(NO_2)$	16.1
C_6H_4(*m*-Cl)	14.5
C_6H_5	16.3
C_6H_4(OMe)	15.4

[a] SMD(ε = 13.6)/B3LYP-D3(BJ)/basis-II//B3LYP-D3(BJ)/basis-I level of theory at 248.15 K. [b] kcal mol^{-1}

19. References

1. Wasilke, J.-C.; Wu, G.; Bu, X.; Kehr, G.; Erker, G. Ruthenium Carbene Complexes Featuring a Tridentate Pincer-type Ligand. *Organometallics* **2005**, *24*, 4289-4297.
2. Donoghue, P. J.; Tehranchi, J.; Cramer, C. J.; Sarangi, R.; Solomon, E. I.; Tolman, W. B. Rapid C–H Bond Activation by a Monocopper(III)–Hydroxide Complex. *J. Am. Chem. Soc.* **2011,** *133*, 17602-17605.
3. Dhar, D.; Yee, G. M.; Spaeth, A. D.; Boyce, D. W.; Zhang, H.; Dereli, B.; Cramer, C. J.; Tolman, W. B. Perturbing the Copper(III)-Hydroxide Unit through Ligand Structural Variation. *J. Am. Chem. Soc.* **2016,** *138*, 356-368.
4. Stoll, S.; Schweiger, A. EasySpin, a comprehensive software package for spectral simulation and analysis in EPR. *J. Magn. Reson.* **2006**, *178*, 42-55.
5. Sheldrick, G. A short history of SHELX. *Acta Cryst. A* **2008**, *64*, 112-122.
6. Mandal, M.; Elwell, C. E.; Bouchey, C. J.; Zerk, T. J.; Tolman, W. B.; Cramer, C. J. "Mechanisms for Hydrogen Atom Abstraction by Mononuclear Copper(III) Cores: HAT or cPCET?" submitted for publication.
7. Tumanov, V. E.; Denisov, E. T. Estimation of the Dissociation Energies of O-O, C-O, and O-H Bonds in Acyl Peroxides, Acids, and Esters from Kinetic Data on the Degradation of Diacyl Peroxides. *Pet. Chem.* **2004**, *45*, 237-248.
8. Luo, Y. R.: *Handbook of Bond Dissociation Energies in Organic Compounds*; CRC Press LLC: Boca Raton, FL, 2003.
9. Gaussian 16, Revision B.01, Frisch, M. J.; Trucks, G. W.; Schlegel, H. B.; Scuseria, G. E.; Robb, M. A.; *et al.* Gaussian, Inc., Wallingford CT, 2016.
10. (a) Becke, A. D. Density-Functional Thermochemistry. III. The Role of Exact Exchange. *J. Chem. Phys.* **1993**, *98*, 5648. (b) Becke, A. D. Density-functional Thermochemistry. IV. A New Dynamical Correlation Functional and Implications for Exact-exchange Mixing. *J. Chem. Phys.* **1996**, *104*, 1040–1046.
11. (a) Grimme, S.; Ehrlich, S.; Goerigk, L. Effect of the Damping Function in Dispersion Corrected Density Functional Theory. *J. Comput. Chem.* **2011**, *32*, 1456–1465. (b) Johnson, E. R.; Becke, A. D. A Post-Hartree-Fock Model of Intermolecular Interactions: Inclusion of Higher-Order Corrections. *J. Chem. Phys.* **2006**, *124*, 174104.

12. Hehre, W. J.; Ditchfield, R.; Pople, J. A. Self—Consistent Molecular Orbital Methods. XII. Further Extensions of Gaussian—Type Basis Sets for Use in Molecular Orbital Studies of Organic Molecules. *J. Chem. Phys.* **1972**, *56*, 2257–2261.
13. Dolg, M.; Wedig, U.; Stoll, H.; Preuss, H. Energy-adjusted Ab Initio Pseudopotentials for the First Row Transition Elements. *J. Chem. Phys.* **1987**, *86*, 866–872.
14. Weigend, F.; Ahlrichs, R. Balanced Basis Sets of Split Valence, Triple Zeta Valence and Quadruple Zeta Valence Quality for H to Rn: Design and Assessment of Accuracy. *Phys. Chem. Chem. Phys.* **2005**, *7*, 3297.
15. Marenich, A. V.; Cramer, C. J.; Truhlar, D. G. Universal Solvation Model Based on Solute Electron Density and on a Continuum Model of the Solvent Defined by the Bulk Dielectric Constant and Atomic Surface Tensions. *J. Phys. Chem. B* **2009**, *113*, 6378–6396.
16. Yamaguchi, K.; Takahara, Y.; Fueno, T.; Houk, K. N. Extended Hartree-Fock (EHF) Theory of Chemical Reactions. *Theor. Chim. Acta* **1988**, *73*, 337–364.
17. Adamo, C.; Barone, V. Toward Reliable Density Functional Methods without Adjustable Parameters: The PBE0 Model. *J. Chem. Phys.* **1999**, *110*, 6158.
18. Marenich, A. V.; Cramer, C. J.; Truhlar, D. G.; Guido, C. A.; Mennucci, B.; Scalmani, G.; Frisch, M. J. Practical Computation of Electronic Excitation in Solution: Vertical Excitation Model. *Chem. Sci.* **2011**, *2*, 2143-2161.